ACS APPLIED MATERIALS & INTERFACES

Research Article

www.acsami.org

Nano- and Microstructures of Magnetic Field-Guided Maghemite Nanoparticles in Diblock Copolymer Films

Yuan Yao,[†] Ezzeldin Metwalli,[†] Martin A. Niedermeier,[†] Matthias Opel,[‡] Chen Lin,[†] Jing Ning,[†] Jan Perlich,[§] Stephan V. Roth,[§] and Peter Müller-Buschbaum*[,†]

[†]Physik-Department, Lehrstuhl für Funktionelle Materialien, Technische Universität München, James-Franck-Str. 1, 85748 Garching, Germany

[‡]Walther-Meissner-Institut, Bayerische Akademie der Wissenschaften, Walther-Meissner-Straße 8, 85748 Garching, Germany

[§]Deutsches Elektronen-Synchrotron DESY, Notkestr. 85, 22603 Hamburg, Germany

Supporting Information

ABSTRACT: The control over the alignment of nanoparticles within a block copolymer matrix was investigated for different external magnetic fields with respect to producing well-aligned, highly oriented metal-oxide−polymer nanopatterns. Hybrid films were prepared by solution casting under a range of external magnetic fields. The nano- and microstructure of maghemite nanoparticles within poly(styrene-*b*-methyl methacrylate) diblock copolymer films as a function of the nanoparticle concentration was studied using optical microscopy, atomic force microscopy, scanning electron microscopy, and grazing incidence small-angle X-ray scattering. Because of a polystyrene (PS) coating, the nanoparticles are incorporated in the PS domains of the diblock copolymer morphology. At higher nanoparticle concentrations, nanoparticle aggregates perturb the block copolymer structure and accumulate at the films surface into wire-shaped stripes. These wire-shaped nanoparticle aggregates form mainly because of the competition between nanoparticle−polymer friction and magnetic dipolar interaction. The magnetic behavior of the hybrid films was probed at different temperatures for two orthogonal directions (with the line-shaped particle aggregates parallel and perpendicular to the magnetic field). The hybrid film systems show superparamagnetic behavior and remarkable shape anisotropy that render them interesting for magnetic applications.

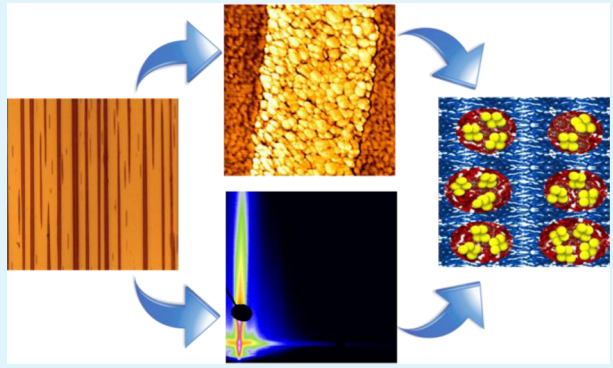

KEYWORDS: *maghemite nanoparticle, GISAXS, block copolymer, thin film, magnetic shape anisotropy, magnetic wires*

1. INTRODUCTION

Hybrid nanocomposites based on a block copolymer matrix and embedded inorganic nanoparticles have attracted great interest because of the potential of tailoring their properties for numerous potential applications. Adding different types of functional nanoparticle fillers endows the hybrid nanocomposites with specific advantageous optical, electric, or magnetic properties, making them interesting materials for various fields of application such as photonic band gap materials, solar cells, sensors, high-frequency loss-free switching, biomedical imaging, medical diagnosis and therapy, catalysis, drug delivery, and high-density magnetic storage devices.[1−24] In general, nanoparticles can have tremendous advantages in their physical and chemical properties because of the large ratio of surface area to volume.[25] In particular, maghemite (γ-Fe_2O_3) nanoparticles have attracted great attention because of their many applications for medical purposes and magnetic storage. Compared to bulk magnetic material, the low magnetic remanence and coercivity of the magnetic nanoparticles are typically beneficial.[26] The control over the alignment of the nanoparticles within the diblock copolymer matrix is essential for producing well-aligned, highly oriented metal-oxide−polymer nanopatterns. This can be achieved using a guiding polymer matrix[27,28] and an external field force, such as an electrical field[29,30] or a magnetic field.[31−33]

The central aim of our investigation was to obtain superparamagnetic films with shape anisotropy from a low-temperature wet-chemical deposition route. This was realized by hybrid films of metal-oxide nanowires and a block copolymer with dispersed nanoparticles. We employed an easy process to create the submicrometer-sized metal-oxide wires and to fine-tune the possible factors controlling the length and width of the formed wires in/on the BC matrix. This investigation was mainly motivated by applications in high-density magnetic information storage and magnetic sensors.

Received: January 27, 2014
Accepted: March 12, 2014
Published: March 12, 2014

Normally, the fabrication of relevant magnetic nano- or micromagnetic wires requires high voltage,[27] high energy costs,[28] high temperature,[29] and so on. We investigated a novel method to fabricate arrays of magnetic metal-oxide wires at room temperature and atmospheric pressure that results in fairly low energy cost. We aimed at an easy single preparation step that leads to a controlled aggregation of magnetic nanoparticles into a defined dimension with the help of the polymer matrix and magnetic field.

Several investigations on the dispersion of magnetic nanoparticles in homopolymers have been reported previously.[34,35] In contrast to homopolymers, block copolymers enhance the system's structural complexity and the formation of hierarchically ordered structures. Consequently, using a block copolymer template together with magnetic nanoparticles allows for different morphologies to be created.[36,37] On one hand, this can be achieved by using a guiding polymer matrix that provides an ordered nanopatterned template for the arrangement of the nanoparticles.[38] On the other hand, the polymer morphology can be also modified via nanoparticle incorporation inside the polymer domains.[39] For example, Lo et al. reported that nanoparticles are well-dispersed in ordered PS domains if the ratio of the nanoparticle diameter, d, to the PS domain size, D, fulfills $d/D < 0.3$.[40] When the nanoparticle size matches or is bigger than the domain size of one block of the block copolymer, a phase transition from a lamella to a cylinder morphology was reported.[40] Wu et al. also reported on the dispersion of magnetic nanoparticles in styrene-butadiene-styrene (SBS) triblock copolymer templates.[41] They found a modification of the morphology of the SBS film by varying the ratio of the particle diameter to the lamella spacing of the PB domains.[41] Lo et al. investigated the organization of pyridine-grafted Fe_2P magnetic nanorods in P(S-*b*-VP) diblock copolymer as a function of the length and concentration of the nanorods.[42] For short nanorod lengths, the particles follow the polymer morphology, whereas for long rod lengths, extensive rod aggregation was observed.[42] Aissou et al. prepared a hybrid thin film consisting of a P(S-*b*-EO) asymmetric diblock copolymer and FePt nanoparticles.[43] A toluene/water solvent annealing process guided the FePt nanoparticles, which were covered with short dopamine-terminated methoxy poly(ethylene oxide) to allow them to be accommodated within the spherical PEO domains.[43]

In the literature, several investigations have been performed that are related to the self-assembly of nanoparticles located inside a block copolymer matrix. However, these investigations are limited to systems with block copolymers acting as a template.[44,45] The majority of research in this field has been focused on embedding the nanoparticles into the templates, which is followed by appropriate treatments to reach an equilibrated structure.[46−49] In the present work, we combined the guiding template approach provided by block copolymers with the application of an external magnetic field. In our work, both the block copolymer matrix and the external field were used for guiding the nanoparticles to form novel structures. We observed hybrid structures on the nano- and microscale. Metal-oxide nanoparticle wires were formed on top of the film in coexistence with a hybrid nanoparticle−polymer matrix underneath. In the literature, 1D chains of superparamagnetic nanoparticles have been reported already.[50−53] For example, Keng et al. investigated 260 nm Pt−Co_3O_4 heterostructures nanowires with polymer-coated ferromagnetic cobalt nanoparticles.[54] Benkoski et al. reported chain-like nanoparticle assemblies of a mixture of 250 nm superparamagnetic magnetite colloids and 24 nm ferromagnetic cobalt nanoparticles.[55] In addition, there are some reports of novel properties resulting from magnetic field-guided magnetic particles material in which the particles sizes are larger than the micrometer scale.[56,57] However, it is well-known that, for cases in which the size of the magnetic nanoparticles is below a single critical magnetic domain size, the magnetic nanoparticles cannot respond to an external magnetic field spontaneously. This is a challenge for the application of very small nanoparticles. To overcome this problem, we selected nanoparticles coated with polystyrene (PS) chains. On one hand, the PS chains allow for a selective incorporation into one domain of the microphase separation structure of the block copolymer matrix and prevent the formation of macroscopic aggregates. On the other hand, as the nanoparticle concentration increases, the likeliness of the nanoparticles to form aggregates increases and thereby nanoparticle aggregates above the critical domain size are formed. Because of these factors, controlled small nanoparticle aggregates start to respond to the external magnetic field and form stripe-like metal-oxide wires that follow the external magnetic lines spontaneously.

So far, we have already investigated several hybrid film systems based on PS-coated iron oxide nanoparticles and different diblock copolymers.[44−46,58−60] These former investigations focused on diblock copolymers that function as structure-directing templates to guide the nanoparticles in the polymer matrix. In the present study, the alignment of maghemite nanoparticles (γ-Fe_2O_3) within poly(styrene-*b*-methylmethacrylate) diblock copolymer films was investigated in an external magnetic field. The morphology and inner (buried) structure of the resulting hybrid films were probed as a function of the external magnetic field strength and for different concentrations of maghemite nanoparticles. The obtained structures were characterized using optical microscopy (OM), atomic force microscopy (AFM), scanning electron microscopy (SEM), and grazing incidence small-angle X-ray scattering (GISAXS). The magnetic behavior of the films was measured at different temperatures for two orthogonal directions: one with the line-shaped particle aggregates oriented parallel to the magnetic field and one with perpendicular orientation.

2. EXPERIMENTAL SECTION

2.1. Sample Preparation. The diblock copolymer poly(styrene-*b*-methyl methacrylate), denoted P(S-*b*-MMA), was purchased from Polymer Source Inc. and used without any further purification. The number average molecular weight of P(S-*b*-MMA) and the weight fraction of PS were 218 kg/mol and 0.15, respectively. The polydispersity was 1.18. According to the polymer interaction parameter, this diblock polymer lies in the strong segregation regime. Maghemite nanoparticles (γ-Fe_2O_3) coated with polystyrene chains were synthesized via a two-step procedure. First, an alkaline solution of iron(II) and iron(III) chloride was mixed with ammonia to pH 9 at room temperature. Magnetite was obtained as spherical 10 nm sized nanoparticles. Then, the solution was acidified and oxidized until the precipitate became brick red, which means that the magnetite has been completely oxidized to maghemite.[61] Second, α-lithium polystyrenesulfonate (LPSS, purchased from Polymer Standards Service, Mainz, Germany) was dissolved in toluene and then added to the acidic aqueous ferrofluid under strong stirring over 30 min at room temperature to obtain the PS-coated maghemite nanoparticles.[61] Details of the nanoparticles synthesis procedure are described elsewhere.[61] The mean diameter of the nanoparticles was 10 nm with a log-normal size distribution (width 0.2). The weight ratio of nanoparticles in toluene solution was 2 wt %.[46] (The chemical identity

and the size of the employed nanoparticles were examined using Mössbauer, XRD, and SAXS measurements. The details are provided in Supporting Information Figures S1−S3.)

Silicon substrates (Si 100, n-type, Silchem) were cut and immersed into an acid cleaning bath (200 mL of H_2SO_4, 70 mL of H_2O_2, and 130 mL of deionized water) at 80 °C for 15 min followed by strong rinsing with deionized water and subsequent drying with N_2 gas.[62] Different nanoparticle−polymer solutions were prepared by using toluene as solvent and having a fixed polymer concentration of 10 mg/mL. The weight ratio of maghemite nanoparticles with respect to the polymer P(S-*b*-MMA) was varied: 50, 25, 15, 8, 3, 1, 0.5, 0.1, and 0.05 wt %. Diblock copolymer films containing magnetic nanoparticles were produced by solution casting on the Si substrates placed horizontally while applying the external magnetic field oriented parallel to the sample surface. Permanent magnets were purchased from Magnet-s4you GmbH. The strength of the applied magnetic field at the center of sample was varied (149, 329, 657, and 1112 G). To obtain solid films, the casting procedure lasted 24 h. All investigated samples in the current study were prepared via the same solution-casting procedure. No further post-treatment steps of the as-cast metal-oxide−polymer hybrid films were employed.

2.2. Surface Structure Characterization. Surface structures were probed with OM, AFM, and SEM. OM was performed using a Zeiss Axiotech 25H microscope at different magnifications. The AFM measurements were done with an Autoprobe CP Research AFM using tapping mode under ambient conditions. Gold-coated Si cantilevers with a spring constant of 2.1 N/m and a resonance frequency of 70 kHz were used. For SEM measurements, an NVision40 FESEM by Carl Zeiss AG was used with an accelerating voltage of 0.4 kV and a working distance of 1 mm.

2.3. Grazing Incidence Small-Angle X-ray Scattering (GISAXS). GISAXS measurements were carried out at beamline P03 of the PETRA III storage ring (DESY, Hamburg, Germany).[63,64] The selected wavelength was $\lambda = 0.0957$ nm. The incident angle was set to $\alpha_i = 0.35°$, which is above the critical angles of all of the materials in the hybrid film system. Therefore, the X-ray beam can penetrate the whole film and give the scattering information through the full depth of the film. The samples were placed horizontally on a sample stage. A sample−detector distance of 2.49 m was used. A beam stop was used to block the direct beam in front of the detector, and a second beam stop was used to block the high-intensity specular reflection to protect the detector from beam damage. A 2D detector (Pilatus 300K with 487 × 619 pixels, pixel size 172 × 172 μm^2) was used for recording the scattering data. Structural information was obtained from horizontal (q_y direction, parallel to the sample surface) and vertical cuts (q_z direction, normal to the sample surface) of the 2D intensity distribution. All samples were measured in two orientations: the X-ray beam was oriented parallel or perpendicular with respect to the wire-shaped nanoparticle aggregates, which were created on top of the hybrid polymer films. Because of the geometry of GISAXS, the horizontal cuts obtained from the direction of the X-ray beam, parallel or perpendicular to the wire-shape aggregates, present the lateral structures perpendicular or parallel to the aggregates, respectively.

2.4. Magnetic Measurements. Direct current (DC) magnetization measurements as a function of temperature were carried out using a superconducting quantum interference device (SQUID) magnetometer (MPMS XL-7, Quantum Design, San Diego, CA, USA). The samples were measured while applying an external magnetic field varied from −350 to 350 mT. The measurements were performed at different temperatures of 2, 3, 4, 5, 10, 20, 50, 100, and 200 K in two orientations: the magnetic nanoparticle wires on the sample were oriented either parallel or perpendicular to the direction of the external magnetic field.

3. RESULTS AND DISCUSSION

Hybrid films with a thickness of 1.5 μm were prepared by mixing the diblock copolymer P(S-*b*-MMA) and the PS-coated maghemite nanoparticles in toluene and a subsequent solution casting on precleaned Si substrates. Maghemite nanoparticles were analyzed to ensure the chemical entity, size, and shape. In contrast to film preparation based on the spin-coating method, solution casting has several advantages. The most important advantage is the relatively slow solvent evaporation, which offers more time for the diblock copolymer film to reach equilibrium with respect to the microphase separation. Moreover, it gives sufficient time to allow for the nanoparticles to respond to the external magnetic field. Second, using solution casting, films with micrometer-scale thicknesses can be easily prepared. Additionally, the solution viscosity, which depends on the polymer concentration, is also an important factor that influences the mobility of the nanoparticles. High viscosities hinder the nanoparticle mobility to some extent because of high friction with the surrounding matrix. For this reason, a low polymer concentration of the solution used for solvent casting (10 mg/mL) was chosen in the present investigation.

3.1. Surface Structures. The microstructures on the sample surface were probed with optical microscopy. Submicrometer- and micrometer-sized wire-shaped nanoparticle aggregates were formed on the film surface. This large-scale surface structure is shown in Figure 1a−d as a function of the nanoparticle concentration. The lines of metal-oxide nanoparticles are oriented along the direction of the external magnetic field (Figure 1a−d). The density of wires per unit surface area as well as the length and width increases with the nanoparticle concentration. Higher nanoparticle concentrations result in an enhancement of the overall system order. The width of the metal-oxide nanowires was determined from the optical micrographs and monotonically increases with the nanoparticle concentration (Figure 1e). At nanoparticle concentrations below 8 wt %, the width of the nanoparticle aggregates is in the range of 0.1−2.5 μm at the applied

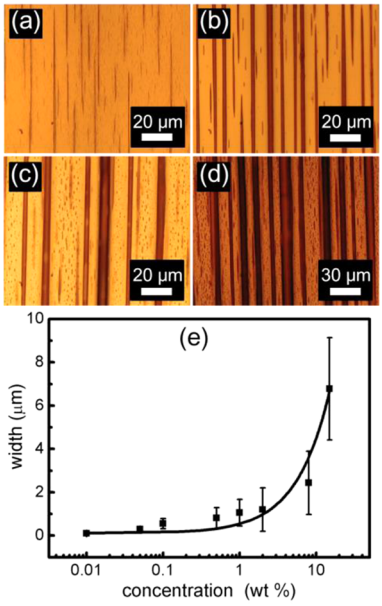

Figure 1. Optical microscopy images of the metal-oxide/polymer hybrid films for a constant applied magnetic field (149 G) with different nanoparticle concentrations: (a) 0.1, (b) 1, (c) 8, and (d) 15 wt %. (e) Extracted widths of the nanoparticle aggregates (wires) as a function of the nanoparticle concentration (the solid line serves as a guide to the eye).

magnetic field of 149 G. For concentrations above 8 wt %, the width strongly increases.

The influence of the magnetic field on the width of the wire-shaped nanoparticle aggregates was investigated as well (Figures 2 and S5). The uniformity of the metal-oxide wires

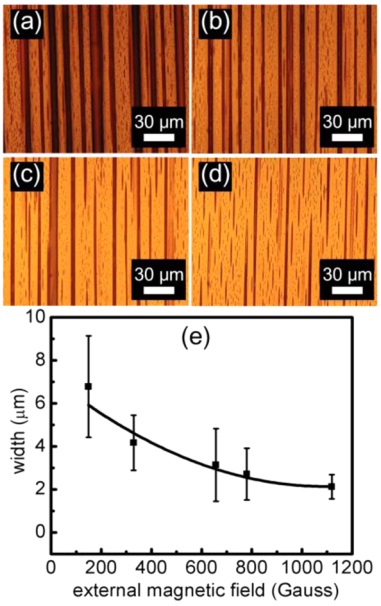

Figure 2. Optical microscopy images of the metal-oxide/polymer hybrid films for a constant nanoparticle concentration (15 wt %) at different external magnetic field strengths: (a) 149, (b) 329, (c) 657, and (d) 1119 G. (e) Extracted widths of the nanoparticle aggregates (wires) as a function of the external magnetic field strength (the solid line serves as a guide to the eye).

width and length is less prominent with the increasing magnetic field strength. The width of the metal-oxide wires decreases with the increasing field strength (Figure 2e). This tendency is caused by the force, F, that is applied from the external magnetic field, H, on the magnetic nanoparticles: $F = mH$. High magnetic forces enhance the mobility of the magnetic nanoparticles in the drying solution and drive them to the macroscopic sample edges. Thus, high forces give rise to aggregation at sample edges instead of dispersing the nanoparticles uniformly inside or on top of the film (see Figure S6). The observations indicate that well-aligned, highly oriented metal-oxide lines can be obtained at low magnetic field strengths, such as 149 G, rather than at higher magnetic fields.

To probe the film's surface morphology in the nanoscale regime, AFM measurements were carried out in tapping mode. Phase images from a selected sample prepared with 3 wt % nanoparticle concentrations at an external applied magnetic field of 149 G are shown in Figure 3. The metal-oxide wires are composed of individual maghemite nanoparticles that are densely packed (Figure 3a,b). Moreover, the formation of the metal-oxide wires involves a limited modification of the polymer morphology.

The microphase separation nanostructure of the diblock copolymer is better displayed in phase images rather than in topography images, particularly in the case of the presence of different materials (here, polymer and metal oxide). The prominent stripe-like metal-oxide wire, small ellipse-like metal aggregates, and dispersed nanoparticles in the PS domains of the P(S-*b*-MMA) diblock copolymer microphase separation

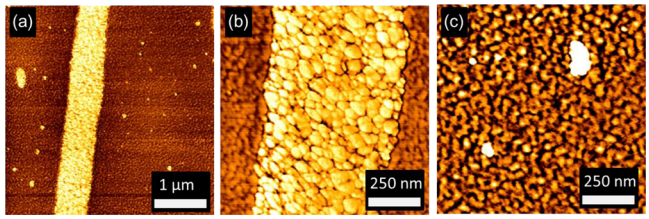

Figure 3. AFM phase images of a selected sample with a 3 wt % nanoparticle concentration under a magnetic field of 149 G: (a) a highly aligned wire-shaped nanoparticle aggregate, (b) the metal-oxide wire is composed of differently sized nanoparticles, and (c) dispersed nanoparticles selectively decorate the microphase-separated diblock copolymer film.

structure are observed in Figure 3. In Figure 3a, the dark parts represent the polymer matrix, whereas the bright parts show the nanoparticles aggregating into a wire. The root-mean-square (rms) roughness is calculated from the corresponding topography AFM data. For the sample with 3 wt % nanoparticle concentration, the value of the rms roughness is below 5 nm in metal-oxide wire-free area. Normally, the rms roughness increases with the increasing concentration of incorporated nanoparticles, but even for high concentrations such as 15 wt %, the rms roughness remains small and was below 10 nm in metal-oxide wire-free areas. The height of the metal-oxide wires is about 7 nm, as revealed from the AFM topographical images. This indicates that the metal-oxide wires are not only supported on the film surface but also partially buried underneath the polymer surface. Additionally, there are several smaller nanoparticle aggregates that form dots of different sizes and are well-dispersed in the polymer matrix (Figure 3b). It is obvious that differently sized nanoparticle aggregates are formed. As a consequence, the metal-oxide wire is an aggregate of nanoparticles of different shapes and sizes. Figure 3c shows the nanostructured diblock copolymer film that originates from microphase separation. Moreover, Figure 3c shows that the individual nanoparticles are selectively embedded within the PS nanodomains. When a large number of nanoparticles are embedded inside the PS domains, these domains start to expand, and ill-defined structures of large nanoparticle aggregates are then formed. After the aggregates have grown above a certain critical size, they respond to the external magnetic field and lead to the formation of metal-oxide wires with high shape anisotropy (Figure 3c).

To confirm the observations obtained with AFM, characterization with SEM was performed. SEM probes surface structures on a larger area of the hybrid film and with a different contrast as compared with AFM. The penetration depth in case of SEM is approximately 10 nm. Thus, SEM shows not only the surface but also the morphology buried within a depth of 10 nm. In the SEM image shown in Figure 4, the dark phase in the polymer matrix is the majority block PMMA, and the second brighter domain is the spherical PS block. The brightest objects are nanoparticles, nanoparticle aggregates, and the very prominent wire-shaped nanoparticle aggregate. A highly ordered spherical microphase separation is clearly observed in the polymer matrix. When the size of the nanoparticle aggregates is smaller than the PS domains, they are located inside the PS spheres and are surrounded by PMMA blocks via a particle−polymer self-assembly process, as explained earlier. The different magnitudes of aggregates show different growth stages before exceeding the critical

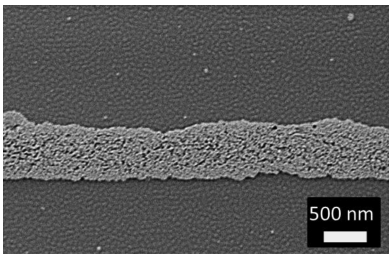

Figure 4. SEM image of a selected sample with a 0.5 wt % nanoparticle concentration prepared at a magnetic field of 149 G.

size. As seen with AFM, the large metal-oxide wire consists of a large number of densely packed nanoparticles.

3.2. Formation of Wire-Shaped Nanoparticle Aggregates. Commonly, a critical magnetic domain size is defined on the basis of the assumption that ferromagnetic materials are composed of magnetic domains.[65] Domains are divided by domain walls, and the magnetic system likes to minimize the net free energy. On one hand, the magnetostatic energy increases proportionally to the volume of the domain; on the other hand, the domain wall energy increases proportionally to the domain surface area. As a result of the competition between these two factors, a critical radius, r_c, is calculated according to[66]

$$r_c \approx 9\frac{(AK_u)^{1/2}}{\mu_0 M_s^2} \quad (1)$$

where A is the exchange constant, K_u is the uniaxial magnetic anisotropy constant, μ_0 is the vacuum permeability, and M_s is the saturation magnetization.

Below this single magnetic domain size, the formation of a magnetic single domain nanoparticle is energetically unfavorable because of the domain wall energy.[67] Above the critical size, the nanoparticles can act as a single magnetic domain.[66] In the case of maghemite, the critical radius is 30 nm.[68] This value is 6 times larger than the size of the nanoparticles used in the present investigation. At the sample preparation temperature, the energy fluctuation originates from thermal energy (k_BT) that may exceed the effective anisotropy energy barrier ($\Delta E_B = KV$, where K is the uniaxial anisotropy constant and V is the particle volume). Thus, the small nanoparticles show superparamagnetic behavior and do not respond to the external applied magnetic field as long as they do not aggregate.

Correspondingly, a three-step process for the magnetic nanoparticles to form large magnetic wires is suggested: (1) In the case of nanoparticles with a size below the critical domain size, the driving force, which originates from microphase separation of the diblock copolymer, exceeds the interaction force between nanoparticles, leading to the nanoparticles swelling the PS domains of the diblock copolymer film. (2) As the nanoparticle concentration increases, the likeliness that the nanoparticles will form aggregates increases and thereby nanoparticle aggregates above the critical domain size are formed. The ordered polymer domains are disrupted by large aggregate formation. (3) The nanoparticle aggregates and large-sized nanoparticles from the tail of the nanoparticle distribution respond to the external magnetic field and form stripe-like metal-oxide wires that follow the external magnetic lines spontaneously.

Generally speaking, the localization of nanoparticles insides the different diblock copolymer domains or at the interfaces between the two blocks results from a competition of entropy and enthalpy. Usually, any localization of the nanoparticles will retard the ordering of the diblock copolymer film because the embedded nanoparticles will change the interaction parameter of the system and increase the entropy penalty, which is energetically unfavorable. Placing nanoparticles coated with PS within the PS domains is enthalpically favored compared with contact to the other block PMMA. The PS coating of the nanoparticles optimizes the interaction parameter between nanoparticles and polymer matrix and even enhances the ordering of the copolymer matrix.[54] In this case, the favorable enthalpic interaction is the primary driving force that guides the localization of PS-coated nanoparticles in the PS domain.

As the nanoparticle concentration increases, the nanoparticles continue to swell the PS domain, and the PS chains continue to stretch to accommodate the nanoparticles. As more particles are incorporated, the entropy penalty dominates, and particles tend to aggregate instead. This causes the highly ordered PS domains to lose their orientation as well to form ill-defined structures. In addition, there is a superexchange interaction between magnetic nanoparticles that are isolated by the insulating polymer matrix. The superexchange interaction can occur via intermediate atoms or ions depending on the structure and the nature of the matrix as well as the bonding at the particle−matrix interface.[69] Because of these two factors, nanoparticles accumulate into aggregates with sizes that exceed the critical magnetic domain size. In other words, the shape anisotropy behavior sets in.

The magnitude of the magnetic nanoparticle moment is proportional to its volume.[67] The large nanoparticle aggregates can be considered as multiple magnetic units and contain thousands of magnetic moments. When nanoparticles form asymmetric aggregates, the hard or easy magnetization axis is created. Magnetic moments have a tendency to align along the longest axis, which defines the direction of shape anisotropy.[70] The shape anisotropy is a dipolar contribution and is calculated by assuming that magnetic poles are distributed uniformly on the surfaces.[67] When nanoparticle aggregates are magnetized by an external magnetic field, the dipole−dipole interaction between particles and the strength of interaction increases with the nanoparticle concentration. Magnetized nanoparticles try to arrange into head-to-tail patterns. The movement of the nanoparticles magnetic moment provides the foremost driving force in the formation of large metal-oxide wires. Within a defined area, as the concentration increases, the mean distances between nanoparticles will decrease. According to[71]

$$E = \left(\frac{\mu_0}{4\pi r^2}\right)\left[\vec{m}_1\vec{m}_1 - \left(\frac{3}{r^2}\right)(\vec{m}_1\vec{r})(\vec{m}_2\vec{r})\right] \quad (2)$$

the dipole−dipole interaction is inversely proportional to the distance vector, r. Thus, the driving force will increase with the concentration because of the reduced nanoparticles interdistance. On the contrary, besides the driving force, several opposing forces exist. First of all, friction occurs everywhere if there is an interface contact between the nanoparticles and polymer matrix, and this is correlated with the metal-oxide nanoparticle concentration. The competition between the dipolar−dipolar attractive force and friction is complex. At higher nanoparticle concentration, the nanoparticle aggregates become larger in size, so the attractive force dominates because it is proportional to the volume of the aggregates. According to the volume equation for spherical particles, $V = 4/3\pi R^3$, the attractive force increases with the third power of the aggregate

radius. However, friction is a resistance force against aggregate mobility, and it depends on the surface area of the aggregates. The friction can be assumed to increase with the square power of the aggregate radius, $A = 4\pi R^2$. In short, increasing nanoparticle concentration strongly contributes to the nanoparticles size growth. This leads to both the dipolar−dipolar attractive force and increased friction, but the driving force from the former increases at a much faster rate than the resistance from the latter. In addition, the wires are highly aligned because of a side-by-side dipolar mutual repulsion as the magnetic moments arrange in the same orientation. Therefore, the nanoparticle concentration is a crucial factor for manipulating the metal-oxide wire's size. In summary, the alignment of the magnetic nanoparticles is a consequence of balancing the driving force of head-to-tail dipolar interaction, resistance of interphase friction, and side-by-side dipolar interaction. Under the influence of these opposing forces, the metal-oxide wire size, width, and spacing to neighboring wires can be tuned.

3.3. Buried Structures Formed Inside the Hybrid Films. The surface and near-surface structures were investigated by AFM and SEM techniques. To study the inner nanostructures located underneath the surface with high statistical relevance, the films were investigated with GISAXS. Details of the GISAXS technique are described elsewhere.[72] All samples were measured in two orientations of the metal-oxide wires with respect to the X-ray beam: parallel or perpendicular. To focus on the nanomorphology, the resolution limit in the GISAXS measurement was chosen such that the metal-oxide wires are not resolved. Thus, the structural information gained with GISAXS is related to the nanoscale size of film morphology (e.g., the microphase separation structure of the polymer film and the nanoparticles).

Figure 5a−d displays selected 2D GISAXS data of samples with different nanoparticle concentrations for the parallel orientation of the X-ray beam with respect to the metal-oxide wires. For all measurements, the specular peak is well-separated from the Yoneda peak (material characteristic position) and is shielded by a beam stop for protecting the detector against the high-intensity specular reflection. Along the vertical direction, structural information normal to the sample surface is obtained. No intensity modulation is observed in the vertical direction (along the q_z direction), which indicates the absence of correlated roughness.[73] The 2D GISAXS patterns change significantly with incorporation of the nanoparticles. Although in the case of the pure polymer film (0 wt %, Figure 5a) side maxima are observed, which correspond to the well-ordered spherical domains of the block copolymer matrix, these maxima vanish upon addition of an extremely small concentration of nanoparticles (0.05 wt %, Figure 5b). Moreover, the intensity in the Yoneda region is more pronounced because of the electron density contrast between γ-Fe_2O_3 and PS/PMMA. The overall shape of the 2D GISAXS patterns remains similar at low nanoparticle concentrations. For higher concentrations, the Yoneda peak broadens, and the overall scattered intensity is enhanced. At 8 wt % nanoparticles, the polymer characteristic scattering signal is lost because of the surface roughness, which apparently increases with increasing nanoparticle concentration.

For quantitative analysis, horizontal line cuts from the 2D GISAXS data were investigated. In Figure 6a, these horizontal line cuts are plotted for the parallel orientation (probing the inner structure perpendicular to the metal-oxide wires) together with fits to the data. Different main features are observed

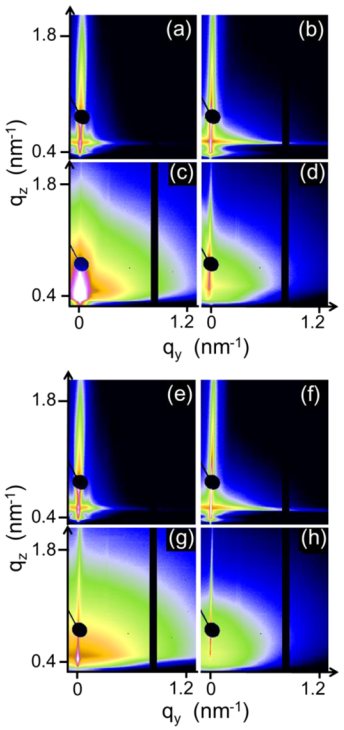

Figure 5. Selected 2D GISAXS data of the metal-oxide−polymer hybrid films with different particle concentrations, with the X-ray beam oriented (a−d) parallel and (e−h) perpendicular to the metal-oxide wires: (a, e) 0, (b, f) 0.05, (c, g) 3, and (d, h) 8 wt %. All images are displayed using the same intensity scale bar as indicated.

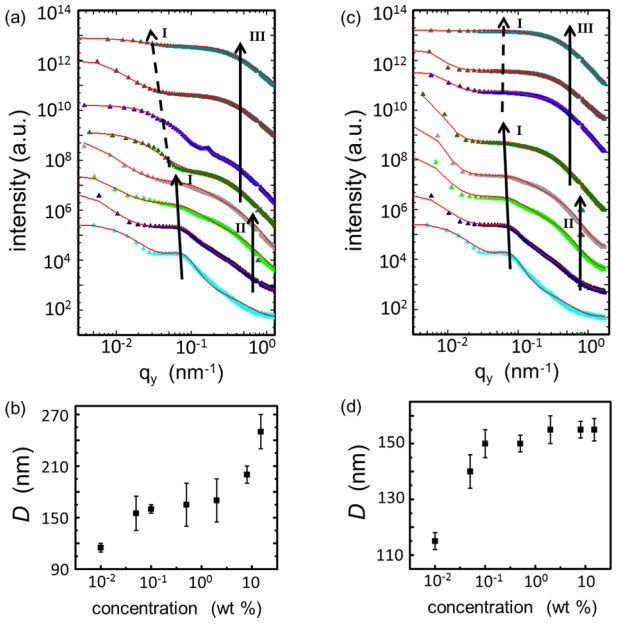

Figure 6. Horizontal line cuts of the 2D GISAXS data (symbols) of the hybrid films with different nanoparticle concentrations (0, 0.01, 0.05, 0.1, 0.5, 3, 8, and 15 wt % from bottom to top) when the X-ray beam is oriented (a) parallel or (b) perpendicular to the metal-oxide wires, which represents the inner structure perpendicular or parallel to the metal-oxide wires, respectively. The curves are shifted for clarity and are shown together with the fits (solid lines). Interdomain distance, D, of the (c) perpendicular and (d) parallel structures plotted as a function of nanoparticle concentration.

dx.doi.org/10.1021/am500597t | ACS Appl. Mater. Interfaces 2014, 6, 5244−5254

(marked as I and II/III). Peak I is located at small q_y values. It is clearly visible for very low nanoparticle concentrations and becomes less pronounced for the films with concentrations above 0.1 wt %. Its position resembles the distance between two neighboring diblock copolymer domains that are created by microphase separation. In the fit, this structure factor is modeled with a Lorentzian distribution function. The corresponding interdomain distance, *D*, which is obtained from peak I, increases from 92 ± 2 to 165 ± 5 nm for the nanoparticle concentrations from 0 to 0.5 wt % (Figure 6b). This increase is attributed to the selective swelling of the PS domains caused by the incorporation of the nanoparticles. As the nanoparticle concentration increases above 0.5 wt %, the intensity of the related peak becomes less prominent, indicating an ill-defined structure of the hybrid film. In other words, the relatively long-range order structure is perturbed because of the overload of the PS domains with nanoparticles. The latter peak progressively shifts to lower q_y values with the increasing metal-oxide content (dashed arrow in Figure 6a). These results reveal the formation of large particle aggregates at high nanoparticle concentrations. Additional broad shoulder-like peaks (peak II or III) show up in the scattering profiles (Figure 6b) and are attributed to the form factor contribution. If the nanoparticle concentration is below 0.5 wt %, the intensity contribution marked with peak II in Figure 6a is perfectly modeled with a form factor contribution of isolated nanoparticles (constant diameter 10 ± 1 nm). Thus, at such low concentrations, the nanoparticles are well-dispersed in the PS domains. At high concentrations, nanoparticle incorporation is no longer selective. Moreover, isolated nanoparticles are no longer dispersed in the polymer matrix. Above a 1 wt % nanoparticle concentration, the scattering is dominated by the form factor of small nanoparticle clusters, which is visible as peak III positioned at q_y values corresponding to 23 ± 1 nm. The position of peak III does not change with increasing nanoparticle concentration (Figure 6a). As a consequence, these small nanoparticle clusters are observed for all block copolymer films with high nanoparticle loading.

Figure 5e–h shows the 2D GISAXS data when the X-ray beam is oriented perpendicular to the metal-oxide wires (probing the inner structure parallel to the metal-oxide wires). In comparison with the 2D GISAXS data of measurements in the parallel orientation, the scattering features are similar at low nanoparticle concentrations. However, at higher nanoparticle concentrations, a remarkable difference is observed: the Yoneda peak intensity is significantly reduced. This reduction originates from the fact that many metal-oxide wires are present on the sample surface for films with a high nanoparticle concentration and these surface structures attenuate the X-ray beam to a certain extent when penetrating the film. Line cuts and fits are shown in Figure 6c. Again, several characteristic structural features are observed. In the case of peak I, its q_y position increases with the nanoparticle concentration for low concentrations, thus showing the same trend as that observed for the parallel orientation (Figure 6a). For high nanoparticle concentrations, peak I stays at a constant q_y position (dashed line in Figure 6c). The corresponding interdomain distance, *D*, extracted from the fitting shows an increase from 92 ± 2 to 155 ± 10 nm followed by regime without further increase (Figure 6d). In addition, the occurrence of isolated nanoparticles (peak II) and small nanoparticle clusters (peak III) is the same for both orientations.

The comparison of the results extracted from the GISAXS data analysis shows that at low nanoparticle concentrations the nanoparticles are well-dispersed inside the PS domains. Consequently, the increase in domain distances in both the parallel and perpendicular orientations is similar. At high nanoparticle concentrations, nanoparticle aggregates have formed that are above the critical size, so they respond to the external magnetic field. As mentioned earlier, the alignment of the magnetic nanoparticles is a consequence of balancing the driving force of head-to-tail dipolar interaction, resistance of interphase friction, and side-by-side dipolar interaction. Because of the fact that the nanoparticles are entangled within the PS chains, those nanoparticles that move and drag the PS domains and cause a morphology change. This acting force perturbs the microphase separation structure and transforms the PS domain structure from a spherical into an elliptical shape, with the long axis oriented perpendicular to the direction of the magnetic field lines. In short, the GISAXS data reveal shape anisotropy on the nanoscale through the whole hybrid film under the influence of an external magnetic field. This shows that the magnetic field also has an effect on the nanostructure of the hybrid film in addition to the formation of micrometer-sized metal-oxide wires that are observed by optical microscopy.

To illustrate the evolution of the morphology on the nanoscale, Figure 7 shows a sketch for different nanoparticle concentrations. The particle-free pure diblock copolymer matrix exhibits a highly ordered, spherical microphase separation morphology. At low nanoparticle concentrations, this ordered structure remains, and the nanoparticles are well-dispersed inside the PS domains, which causes a swelling of the interdomain distance. At moderate nanoparticle concentrations, some small clusters have formed that still can be accommodated inside the PS domains. At high nanoparticle concentrations, the ordered structure is perturbed, and the morphology becomes anisotropic. At nanoparticle concentrations above 0.5 wt %, the block copolymer template structure is deformed, and large wire-shaped nanoparticle aggregates are formed (not shown in Figure 7 because they are on another scale). The resulting film structure is a balance that comes from competition among several factors, such as the driving force from the external magnetic field, repulsion from the large magnetic metallic wires, friction between the polymer matrix, and magnetic dipolar interaction.

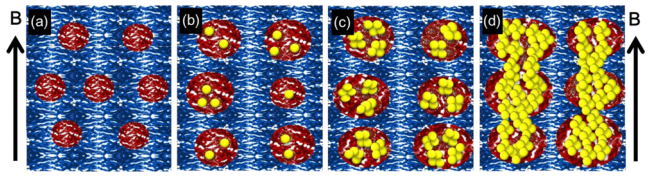

Figure 7. Sketch of polymer–nanoparticle hybrid films for (a) the particle-free pure diblock copolymer film and (b) low, (c) moderate, and (d) high nanoparticle concentrations. The PS block is drawn in red, the PMMA block, in blue, and the maghemite nanoparticles, in yellow. The direction of the magnetic field is indicated by the black arrows.

3.4. Magnetic Properties. Magnetic properties of the polymer–nanoparticle hybrid films were investigated using SQUID magnetometry (Quantum Design MPMS) with the external magnetic field applied parallel or perpendicular to the magnetic wires.

From the parallel orientation measurements (Figure 8a) of the magnetic moment at different temperatures for the sample

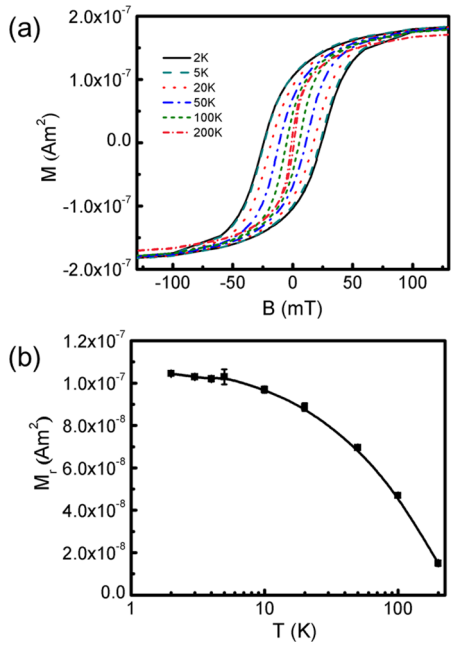

Figure 8. (a) Magnetic moments measured as a function of the external magnetic field with a parallel orientation at different temperatures for a selected sample with 0.1 wt % nanoparticles. (b) Temperature dependence of the measured remanence of the selected sample with 0.1 wt % nanoparticles.

with 0.1 wt %, it is observed that the saturation magnetization is temperature-independent. With increasing temperature, the coercive fields become much smaller because of thermal agitation. Magnetic hysteresis is present for temperatures that are below a characteristic temperature. This is typical superparamagnetic behavior, and the characteristic temperature can be identified with the blocking temperature of superparamagnetic particles, which is raised by the Néel–Brown expression[74,75]

$$\tau = \tau_0 \exp\left(\frac{KV}{k_B T}\right) \quad (3)$$

where $\tau_0 \approx 10^{-10}$ s is the inverse attempt frequency, τ is the relaxation time, $k_B T$ is the thermal energy, K is the uniaxial anisotropy, V is the particle volume, and KV then yields the activation energy. In addition, these magnetization curves superimpose and exhibit a temperature dependence. The remanence, which originates from the measured magnetic moment curves (Figure 8a), is temperature-dependent (Figure 8b). Within experimental error, the remanence stays constant with small fluctuations at low temperatures and reduces strongly at higher temperatures.

Figure 9a shows magnetization curves at T = 2 K for all investigated nanoparticle concentrations, again with the magnetic field applied parallel to the metal wires. To analyze the data, the remanence, M_r, saturation magnetization, M_s, and relative remanence, M_r/M_s, are plotted as a function of the nanoparticles concentration in Figure 9b. Within experimental error, both M_r and M_s increase linearly with concentration. In contrast, the relative remanence remains constant irrespective of concentration. Taking into account all of the results above,

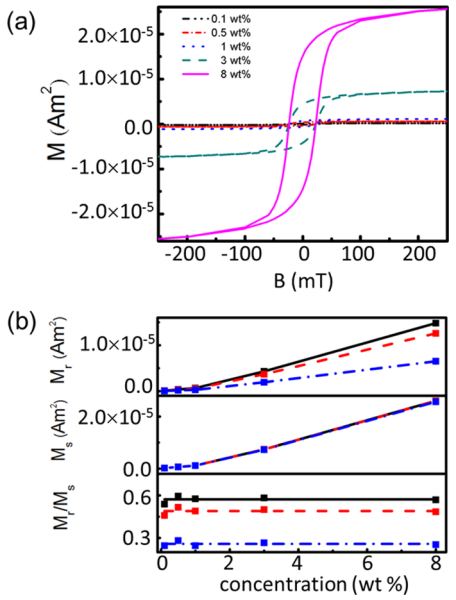

Figure 9. (a) Magnetic moments measured as a function of the external magnetic field at 2 K with nanoparticle concentrations of 0.1, 0.5, 1, 3, and 8 wt %. (b) Nanoparticle concentration dependence of the remanence, M_r, saturation magnetization, M_s, and relative remanence, M_r/M_s, at 2 (black solid line), 20 (red dashed line), 100 K (blue dashed-dotted line).

the hybrid film system matches the requirements of superparamagnetic materials,[76] proving that the nanoparticles in the hybrid film system have not lost the magnetic character of nanosize particles. The behavior can be explained well in the Stoner–Wohlfarth–Néel model.[74,75]

Additional hysteresis loops were measured at 2 K with the applied magnetic field parallel or perpendicular to the metal wires (Figure 10). The results show that the sample is easier to

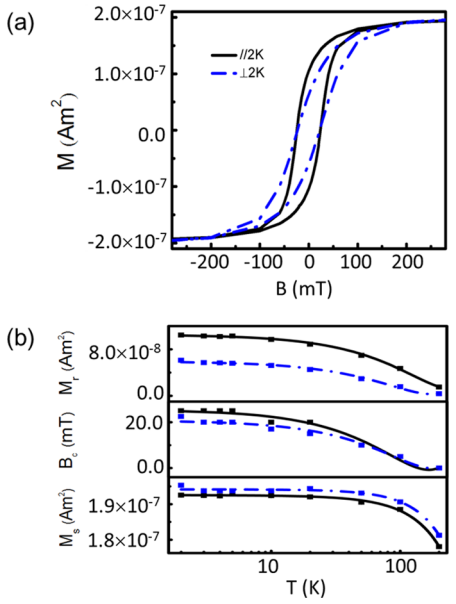

Figure 10. (a) Magnetic moment curves and (b) temperature dependence of the remanence, coercivity, and saturation magnetization measured at 2 K with a parallel (black solid line) and perpendicular (blue dashed-dotted line) external magnetic field orientation.

dx.doi.org/10.1021/am500597t | ACS Appl. Mater. Interfaces 2014, 6, 5244–5254

magnetize along the metal wires direction than in the perpendicular direction. Within experimental error, the remanence, coercivity, and saturation magnetization have strong, weak, and no orientation dependence, respectively (Figure 10b). This indicates that the direction along the metal-oxide wires is the easy magnetization axis and the perpendicular direction is the hard magnetization axis. The long-range magnetic order mainly depends on mutually aligning the dipolar field of the nanoparticles, which leads the magnetization to follow the polar direction along the easy direction, invoking quantum mechanical superexchange.[77,78] Compared with the magnetically isotropic property of metal−polymer nanocomposite films reported in our previous investigation[46] in which the nanoparticles were highly dispersed in the diblock copolymer film, an obvious unique magnetic anisotropy is observed for the prepared samples under an external magnetic field because of the formation of magnetic wires.

4. CONCLUSIONS

Superparamagnetic films with shape anisotropy were obtained from a low-temperature wet-chemical deposition route. The hybrid films of PS-coated γ-Fe_2O_3 nanoparticles in a P(*S*-*b*-MMA) diblock copolymer matrix with highly oriented wire-shaped nanoparticle aggregates on top were investigated using OM, AFM, SEM, and GISAXS. By tuning the nanoparticle concentration and the strength of an external magnetic field applied during preparation, the corresponding highly oriented metal-oxide wires with different widths, lengths, and spacing were prepared. Diblock copolymer films provide ordered nanostructures via a microphase separation process and act as a template material for guiding the incorporated nanoparticles. The PS-coated nanoparticles were selectively deposited into the PS domains at low concentrations. At high nanoparticle concentrations, metal-oxide aggregates were formed that reach the single magnetic domain critical size. Thereafter, nanoparticle aggregates were magnetized and driven by a head-to-tail dipolar−dipolar attractive interaction to align and form long stripes of metal-oxide wires along the direction of the external magnetic field. In addition, the polymer nanomorphology was changed from symmetrical to asymmetrical because of the movement of nanoparticles within the polymer film. As a consequence, the structure of the hybrid film is highly anisotropic, both on the microscale as well as on the nanoscale. These findings are consistent from both real-space and reciprocal-space measurements. Magnetic measurements were collected using SQUID magnetometry. The magnetic results reveal that the hybrid film shows superparamagnetic behavior and strong shape anisotropy. The simple tuning of the magnetic wire widths, lengths, and spacing by manipulating both the nanoparticles concentration and the external applied magnetic field could make this model system highly desirable for many important applications in high-density magnetic information storage and magnetic sensors.

■ ASSOCIATED CONTENT

Supporting Information

Additional experimental results including SAXS, XRD, and Mössbauer spectra of maghemite (γ-Fe_2O_3) nanoparticles; SAXS data of the particle-free block copolymer; optical microscopy images of the metal−polymer hybrid film at the center and edge of the samples; optical microscopy images of the hybrid film prepared with and without an external applied magnetic field; and SEM/EDX of one selected hybrid film. This material is available free of charge via the Internet at http://pubs.acs.org.

■ AUTHOR INFORMATION

Corresponding Author

*E-mail: muellerb@ph.tum.de; Phone: +49 89 289 12451; Fax: +49 89 289 12 473.

Notes

The authors declare no competing financial interest.

■ ACKNOWLEDGMENTS

This work was supported by BMBF (German Ministry of Research and Education) grant no. 03DU03MU. Y.Y. acknowledges the China Scholarship Council (CSC) and C.L. and J.N. acknowledge the Erasmus Mundus scholarship "MaMaSelf" program for funding. We thank Prof. Friedrich E. Wagner for his help with the Mössbauer measurements. We thank Dr. Himendra Jha for his help with the EDX measurements. Portions of this research were carried out at synchrotron light source PETRA III at DESY. DESY is a member of the Helmholtz Association (HGF).

■ REFERENCES

(1) Yoon, J.; Lee, W.; Thomas, E. L. Self-Assembly of Block Copolymers for Photonic-Bandgap Materials. *MRS Bull.* **2005**, *30*, 721−726.

(2) Liao, H.-C.; Tsao, C.-S.; Lin, T.-H.; Jao, M.-H.; Chuang, C.-M.; Chang, S.-Y.; Huang, Y.-C.; Shao, Y.-T.; Chen, C.-Y.; Su, C.-J.; Jeng, U.-S.; Chen, Y.-F.; Su, W.-F. Nanoparticle-Tuned Self-Organization of a Bulk Heterojunction Hybrid Solar Cell with Enhanced Performance. *ACS Nano* **2012**, *6*, 1657−1666.

(3) Rawolle, M.; Niedermeier, M. A.; Kaune, G.; Perlich, J.; Lellig, P.; Memesa, M.; Cheng, Y.-J.; Gutmann, J. S.; Müller-Buschbaum, P. Fabrication and Characterization of Nanostructured Titania Films with Integrated Function from Inorganic−Organic Hybrid Materials. *Chem. Soc. Rev.* **2012**, *41*, 5131−5142.

(4) Krishnamoorthy, S.; Krishnan, S.; Thoniyot, P.; Low, H. Y. Inherently Reproducible Fabrication of Plasmonic Nanoparticle Arrays for SERS by Combining Nanoimprint and Copolymer Lithography. *ACS Appl. Mater. Interfaces* **2011**, *3*, 1033−1040.

(5) Han, E.; Leolukman, M.; Kim, M.; Gopalan, P. Resist Free Patterning of Nonpreferential Buffer Layers for Block Copolymer Lithography. *ACS Nano* **2010**, *4*, 6527−6534.

(6) Ren, S.; Chang, L.-Y.; Lim, S.-K.; Zhao, J.; Smith, M.; Zhao, N.; Bulović, V.; Bawendi, M.; Gradeččak, S. Inorganic−Organic Hybrid Solar Cell: Bridging Quantum Dots to Conjugated Polymer Nanowires. *Nano Lett.* **2011**, *11*, 3998−4002.

(7) Zhao, L.; Loy, D. A.; Shea, K. J. Photodeformable Spherical Hybrid Nanoparticles. *J. Am. Chem. Soc.* **2006**, *128*, 14250−14251.

(8) Patel, R. N.; Heitsch, A. T.; Hyun, C.; Smilgies, D.-M.; de Lozanne, A.; Loo, Y.-L.; Korgel, B. A. Printed Magnetic FePt Nanocrystal Films. *ACS Appl. Mater. Interfaces* **2009**, *1*, 1339−1346.

(9) Chen, H.; Wu, X.; Duan, H.; Wang, Y. A.; Wang, L.; Zhang, M.; Mao, H. Biocompatible Polysiloxane-Containing Diblock Copolymer PEO-*b*-PγMPS for Coating Magnetic Nanoparticles. *ACS Appl. Mater. Interfaces* **2009**, *1*, 2134−2140.

(10) Sukhov, A.; Berakdar, J. Local Control of Ultrafast Dynamics of Magnetic Nanoparticles. *Phys. Rev. Lett.* **2009**, *102*, 057204-1−057204-4.

(11) Yap, F. L.; Thoniyot, P.; Krishnan, S.; Krishnamoorthy, S. Nanoparticle Cluster Arrays for High-Performance SERS through Directed Self-Assembly on Flat Substrates and on Optical Fibers. *ACS Nano* **2012**, *6*, 2056−2070.

(12) Wei, Q.; Lin, Y.; Anderson, E. R.; Briseno, A. L.; Gido, S. P.; Watkins, J. J. Additive-Driven Assembly of Block Copolymer−

Nanoparticle Hybrid Materials for Solution Processable Floating Gate Memory. *ACS Nano* **2012**, *6*, 1188−1194.
(13) Choi, J. H.; Nguyen, F. T.; Barone, P. W.; Heller, D. A.; Moll, A. E.; Patel, D.; Boppart, S. A.; Strano, M. S. Multimodal Biomedical Imaging with Asymmetric Single-Walled Carbon Nanotube/Iron Oxide Nanoparticle Complexes. *Nano Lett.* **2007**, *7*, 861−867.
(14) Mistark, P. A.; Park, S.; Yalcin, S. E.; Lee, D. H.; Yavuzcetin, O.; Tuominen, M. T.; Russell, T. P.; Achermann, M. Block-Copolymer-Based Plasmonic Nanostructures. *ACS Nano* **2009**, *3*, 3987−3992.
(15) Gao, J.; Gu, H.; Xu, B. Multifunctional Magnetic Nanoparticles: Design, Synthesis, and Biomedical Applications. *Acc. Chem. Res.* **2009**, *42*, 1097−1107.
(16) Sknepnek, R.; Anderson, J. A.; Lamm, M. H.; Schmalian, J. r.; Travesset, A. Nanoparticle Ordering via Functionalized Block Copolymers in Solution. *ACS Nano* **2008**, *2*, 1259−1265.
(17) Caruso, F.; Caruso, R. A.; Möhwald, H. Nanoengineering of Inorganic and Hybrid Hollow Spheres by Colloidal Templating. *Science* **1998**, *282*, 1111−1114.
(18) Slowing, I. I.; Trewyn, B. G.; Giri, S.; Lin, V. Y. Mesoporous Silica Nanoparticles for Drug Delivery and Biosensing Applications. *Adv. Func. Mater.* **2007**, *17*, 1225−1236.
(19) Rider, D. A.; Liu, K.; Eloi, J.-C.; Vanderark, L.; Yang, L.; Wang, J.-Y.; Grozea, D.; Lu, Z.-H.; Russell, T. P.; Manners, I. Nanostructured Magnetic Thin Films from Organometallic Block Copolymers: Pyrolysis of Self-Assembled Polystyrene-*block*-Poly(ferrocenylethylmethylsilane). *ACS Nano* **2008**, *2*, 263−270.
(20) Mornet, S.; Vasseur, S.; Grasset, F.; Duguet, E. Magnetic Nanoparticle Design for Medical Diagnosis and Therapy. *J. Mater. Chem.* **2004**, *14*, 2161−2175.
(21) Kruis, F. E.; Fissan, H.; Peled, A. Synthesis of Nanoparticles in the Gas Phase for Electronic, Optical and Magnetic Applications—a Review. *J. Aerosol Sci.* **1998**, *29*, 511−535.
(22) Kim, D. H.; Wei, A.; Won, Y.-Y. Preparation of Super-Stable Gold Nanorods via Encapsulation into Block Copolymer Micelles. *ACS Appl. Mater. Interfaces* **2012**, *4*, 1872−1877.
(23) Budgin, A. M.; Kabachii, Y. A.; Shifrina, Z. B.; Valetsky, P. M.; Kochev, S. S.; Stein, B. D.; Malyutin, A.; Bronstein, L. M. Functionalization of Magnetic Nanoparticles with Amphiphilic Block Copolymers: Self-Assembled Thermoresponsive Submicrometer Particles. *Langmuir* **2012**, *28*, 4142−4151.
(24) Sahoo, B.; Devi, K. S. P.; Banerjee, R.; Maiti, T. K.; Pramanik, P.; Dhara, D. Thermal and pH Responsive Polymer-Tethered Multifunctional Magnetic Nanoparticles for Targeted Delivery of Anticancer Drug. *ACS Appl. Mater. Interfaces* **2013**, *5*, 3884−3893.
(25) Sohn, B. H.; Cohen, R. E. Processible Optically Transparent Block Copolymer Films Containing Superparamagnetic Iron Oxide Nanoclusters. *Chem. Mater.* **1997**, *9*, 264−269.
(26) Lu, A. H.; Salabas, E. L.; Schüth, F. Magnetic Nanoparticles: Synthesis, Protection, Functionalization, and Application. *Angew. Chem., Int. Ed.* **2007**, *46*, 1222−1244.
(27) Schlage, K.; Couet, S.; Roth, S.; Vainio, U.; Rüffer, R.; Kashem, M. A.; Müller-Buschbaum, P.; Röhlsberger, R. The Formation and Magnetism of Iron Nanostructures on Ordered Polymer Templates. *New J. Phys.* **2012**, *14*, 043007.
(28) Jiao, Y.; Akcora, P. Assembly of Polymer-Grafted Magnetic Nanoparticles in Polymer Melts. *Macromolecules* **2012**, *45*, 3463−3470.
(29) Varga, Z.; Filipcsei, G.; Szilágyi, A.; Zrínyi, M. Electric and Magnetic Field-Structured Smart Composites. *Macromol. Symp.* **2005**, *227*, 123−134.
(30) Tomer, V.; Randall, C.; Polizos, G.; Kostelnick, J.; Manias, E. High-and Low-Field Dielectric Characteristics of Dielectrophoretically Aligned Ceramic/Polymer Nanocomposites. *J. Appl. Phys.* **2008**, *103*, 034115−034117.
(31) Fang, W.-X.; He, Z.-H.; Xu, X.-Q.; Mao, Z.-Q.; Shen, H. Magnetic-Field-Induced Chain-Like Assembly Structures of Fe_3O_4 Nanoparticles. *Europhys. Lett.* **2007**, *77*, 68004.
(32) Martin, J. E.; Venturini, E.; Odinek, J.; Anderson, R. A. Anisotropic Magnetism in Field-Structured Composites. *Phys. Rev. E* **2000**, *61*, 2818−2830.
(33) Filipcsei, G.; Csetneki, I.; Szilágyi, A.; Zrínyi, M. In *Oligomers, Polymer Composites, Molecular Imprinting*; Boutevin, B., Ed.; Springer: New York, 2007; pp 137−189, Chapter 104.
(34) Robbes, A.-S.; Jestin, J.; Meneau, F.; Dalmas, F.; Sandre, O.; Perez, J.; Boué, F.; Cousin, F. Homogeneous Dispersion of Magnetic Nanoparticles Aggregates in a PS Nanocomposite: Highly Reproducible Hierarchical Structure Tuned by the Nanoparticles' Size. *Macromolecules* **2010**, *43*, 5785−5796.
(35) Xu, C.; Ohno, K.; Ladmiral, V.; Composto, R. J. Dispersion of Polymer-Grafted Magnetic Nanoparticles in Homopolymers and Block Copolymers. *Polymer* **2008**, *49*, 3568−3577.
(36) Fernandes, N. J.; Koerner, H.; Giannelis, E. P.; Vaia, R. A. Hairy Nanoparticle Assemblies as One-Component Functional Polymer Nanocomposites: Opportunities and Challenges. *MRS Commun.* **2013**, *3*, 13−29.
(37) Metwalli, E.; Körstgens, V.; Schlage, K.; Meier, R.; Kaune, G.; Buffet, A.; Couet, S.; Roth, S. V.; Röhlsberger, R.; Müller-Buschbaum, P. Cobalt Nanoparticles Growth on a Block Copolymer Thin Film: A Time-Resolved GISAXS Study. *Langmuir* **2013**, *29*, 6331−6340.
(38) Hickey, R. J.; Haynes, A. S.; Kikkawa, J. M.; Park, S.-J. Controlling the Self-Assembly Structure of Magnetic Nanoparticles and Amphiphilic Block-Copolymers: From Micelles to Vesicles. *J. Am. Chem. Soc.* **2011**, *133*, 1517−1525.
(39) Raman, V.; Bose, A.; Olsen, B. D.; Hatton, T. A. Long-Range Ordering of Symmetric Block Copolymer Domains by Chaining of Superparamagnetic Nanoparticles in External Magnetic Fields. *Macromolecules* **2012**, *45*, 9373−9382.
(40) Lo, C.-T.; Chang, Y.-C.; Wu, S.-C.; Lee, C.-L. Effect of Particle Size on the Phase Behavior of Block Copolymer/Nanoparticle Composites. *Colloids Surf., A* **2010**, *368*, 6−12.
(41) Wu, J.; Li, H.; Wu, S.; Huang, G.; Xing, W.; Tang, M.; Fu, Q. Influence of Magnetic Nanoparticle Size on the Particle Dispersion and Phase Separation in an ABA Triblock Copolymer. *J. Phys. Chem. B* **2014**, *118*, 2186−2193.
(42) Lo, C.-T.; Lin, W.-T. Effect of Rod Length on the Morphology of Block Copolymer/Magnetic Nanorod Composites. *J. Phys. Chem. B* **2013**, *117*, 5261−5270.
(43) Aissou, K.; Alnasser, T.; Pecastaings, G.; Goglio, G.; Toulemonde, O.; Mornet, S.; Fleury, G.; Hadziioannou, G. Hierarchical Assembly of Magnetic $L1_0$-Ordered FePt Nanoparticles in Block Copolymer Thin Films. *J. Mater. Chem. C* **2013**, *1*, 1317−1321.
(44) Abul Kashem, M. M.; Perlich, J.; Diethert, A.; Wang, W.; Memesa, M.; Gutmann, J. S.; Majkova, E.; Capek, I.; Roth, S. V.; Petry, W.; Müller-Buschbaum, P. Array of Magnetic Nanoparticles via Particle Co-operated Self-Assembly in Block Copolymer Thin Film. *Macromolecules* **2009**, *42*, 6202−6208.
(45) Abul Kashem, M.; Perlich, J.; Schulz, L.; Roth, S.; Petry, W.; Müller-Buschbaum, P. Maghemite Nanoparticles on Supported Diblock Copolymer Nanostructures. *Macromolecules* **2007**, *40*, 5075−5083.
(46) Xia, X.; Metwalli, E.; Ruderer, M. A.; Körstgens, V.; Busch, P.; Böni, P.; Müller-Buschbaum, P. Nanostructured Diblock Copolymer Films with Embedded Magnetic Nanoparticles. *J. Phys.: Condens. Matter* **2011**, *23*, 254203.
(47) Spontak, R. J.; Shankar, R.; Bowman, M. K.; Krishnan, A. S.; Hamersky, M. W.; Samseth, J.; Bockstaller, M. R.; Rasmussen, K. Selectivity- and Size-Induced Segregation of Molecular and Nanoscale Species in Microphase-Ordered Triblock Copolymers. *Nano Lett.* **2006**, *6*, 2115−2120.
(48) Zhao, Y.; Thorkelsson, K.; Mastroianni, A. J.; Schilling, T.; Luther, J. M.; Rancatore, B. J.; Matsunaga, K.; Jinnai, H.; Wu, Y.; Poulsen, D.; Fréchet, J. M. J.; Alivisatos, A. P.; Xu, T. Small-Molecule-Directed Nanoparticle Assembly Towards Stimuli-Responsive Nanocomposites. *Nat. Mater.* **2009**, *8*, 979−985.

(49) Thorkelsson, K.; Mastroianni, A. J.; Ercius, P.; Xu, T. Direct Nanorod Assembly Using Block Copolymer-Based Supramolecules. *Nano Lett.* **2011**, *12*, 498−504.
(50) Singh, H.; Laibinis, P. E.; Hatton, T. A. Synthesis of Flexible Magnetic Nanowires of Permanently Linked Core-Shell Magnetic Beads Tethered to a Glass Surface Patterned by Microcontact Printing. *Nano Lett.* **2005**, *5*, 2149−2154.
(51) Sheparovych, R.; Sahoo, Y.; Motornov, M.; Wang, S.; Luo, H.; Prasad, P. N.; Sokolov, I.; Minko, S. Polyelectrolyte Stabilized Nanowires from Fe_3O_4 Nanoparticles via Magnetic Field Induced Self-Assembly. *Chem. Mater.* **2006**, *18*, 591−593.
(52) Klokkenburg, M.; Vonk, C.; Claesson, E. M.; Meeldijk, J. D.; Erné, B. H.; Philipse, A. P. Direct Imaging of Zero-Field Dipolar Structures in Colloidal Dispersions of Synthetic Magnetite. *J. Am. Chem. Soc.* **2004**, *126*, 16706−16707.
(53) Furst, E. M.; Suzuki, C.; Fermigier, M.; Gast, A. P. Permanently Linked Monodisperse Paramagnetic Chains. *Langmuir* **1998**, *14*, 7334−7336.
(54) Keng, P. Y.; Bull, M. M.; Shim, I.-B.; Nebesny, K. G.; Armstrong, N. R.; Sung, Y.; Char, K.; Pyun, J. Colloidal Polymerization of Polymer-Coated Ferromagnetic Cobalt Nanoparticles into Pt-Co_3O_4 Nanowires. *Chem. Mater.* **2011**, *23*, 1120−1129.
(55) Benkoski, J. J.; Breidenich, J. L.; Uy, O. M.; Hayes, A. T.; Deacon, R. M.; Land, H. B.; Spicer, J. M.; Keng, P. Y.; Pyun, J. Dipolar Organization and Magnetic Actuation of Flagella-Like Nanoparticle Assemblies. *J. Mater. Chem.* **2011**, *21*, 7314−7325.
(56) Nguyen, V. Q.; Ramanujan, R. Novel Coiling Behavior in Magnet-Polymer Composites. *Chem. Phys.* **2010**, *211*, 618−626.
(57) Varga, Z.; Filipcsei, G.; Zrínyi, M. Magnetic Field Sensitive Functional Elastomers with Tuneable Elastic Modulus. *Polymer* **2006**, *47*, 227−233.
(58) Schulz, L.; Schirmacher, W.; Omran, A.; Shah, V.; Böni, P.; Petry, W.; Müller-Buschbaum, P. Elastic Torsion Effects in Magnetic Nanoparticle Diblock-Copolymer Structures. *J. Phys.: Condens. Matter* **2010**, *22*, 346008.
(59) Lauter-Pasyuk, V.; Lauter, H.; Gordeev, G.; Müller-Buschbaum, P.; Toperverg, B.; Petry, W.; Jernenkov, M.; Petrenko, A.; Aksenov, V. Parallel and Perpendicular Lamellar Phases in Copolymer−Nanoparticle Multilayer Structures. *Phys. B* **2004**, *350*, E939−E942.
(60) Lauter-Pasyuk, V.; Lauter, H.; Gordeev, G.; Müller-Buschbaum, P.; Toperverg, B.; Jernenkov, M.; Petry, W. Nanoparticles in Block-Copolymer Films Studied by Specular and Off-Specular Neutron Scattering. *Langmuir* **2003**, *19*, 7783−7788.
(61) Cabuil, V.; Hochart, N.; Perzynski, R.; Lutz, P. J. In *Trends in Colloid and Interface Science VIII*; Ottewill, R. H., Rennie, A. R., Eds.; Springer-Verlag: New York, 1994; pp 71−74, Chapter 15.
(62) Metwalli, E.; Moulin, J.-F.; Perlich, J.; Wang, W.; Diethert, A.; Roth, S.; Muller-Buschbaum, P. Polymer-Template-Assisted Growth of Gold Nanowires Using a Novel Flow-Stream Technique. *Langmuir* **2009**, *25*, 11815−11821.
(63) Rawolle, M.; Körstgens, V.; Ruderer, M.; Metwalli, E.; Guo, S.; Herzog, G.; Benecke, G.; Schwartzkopf, M.; Buffet, A.; Perlich, J.; Roth, S. V.; Müller-Buschbaum, P. Comparison of Grazing Incidence Small Angle X-Ray Scattering of a Titania Sponge Structure at the Beamlines BW4 (DORIS III) and P03 (PETRA III). *Rev. Sci. Instrum.* **2012**, *83*, 106104.
(64) Buffet, A.; Rothkirch, A.; Dohrmann, R.; Korstgens, V.; Abul Kashem, M. M.; Perlich, J.; Herzog, G.; Schwartzkopf, M.; Gehrke, R.; Müller-Buschbaum, P. P03, the Microfocus and Nanofocus X-Ray Scattering (MiNaXS) Beamline of the PETRA III Storage Ring: The Microfocus Endstation. *J. Synchroton Radiat.* **2012**, *19*, 647−653.
(65) Weiss, P. L'hypothèse du Champ Moléculaire et la Propriété Ferromagnétique. *J. Phys. Radium* **1907**, *6*, 661−690.
(66) O'Handley, R. C. *Modern Magnetic Materials: Principles and Applications*; Wiley: New York, 2000.
(67) Bedanta, S.; Kleemann, W. Supermagnetism. *J. Phys. D: Appl. Phys.* **2009**, *42*, 013001.
(68) Givord, D.; Lu, Q.; Rossignol, M. In *Science and Technology of Nanostructured Magnetic Materials*; Hadjipanayis, G., Prinz, G., Eds.; Plenum Press: New York, 1991; pp 635−656.
(69) Chikazumi, S.; Charap, S. *Physics of Magnetism*; RE Krieger Publishing Company: Huntington, NY, 1978.
(70) Stoner, E. C.; Wohlfarth, E. A Mechanism of Magnetic Hysteresis in Heterogeneous Alloys. *Philos. Trans. R. Soc., A* **1948**, 599−642.
(71) Blundell, S. *Magnetism in Condensed Matter*; Oxford University Press: New York, 2001.
(72) Müller-Buschbaum, P. Grazing Incidence Small-Angle X-ray Scattering: An Advanced Scattering Technique for the Investigation of Nanostructured Polymer Films. *Anal. Bioanal. Chem.* **2003**, *376*, 3−10.
(73) Müller-Buschbaum, P.; Stamm, M. Correlated Roughness, Long-Range Correlations, and Dewetting of Thin Polymer Films. *Macromolecules* **1998**, *31*, 3686−3692.
(74) Néel, L. Théorie du Traînage Magnétique des Ferromagnétiques en Grains Fins Avec Applications Aux Terres Cuites. *Ann. Géophys* **1949**, *5*, 99−136.
(75) Brown, W. F., Jr. Thermal Fluctuations of a Single-Domain Particle. *Phys. Rev.* **1963**, *130*, 1677.
(76) Bean, C. P.; Jacobs, I. S. Magnetic Granulometry and Super-Paramagnetism. *J. Appl. Phys.* **1956**, *27*, 1448−1452.
(77) Scheinfein, M.; Schmidt, K.; Heim, K.; Hembree, G. Magnetic Order in Two-Dimensional Arrays of Nanometer-Sized Superparamagnets. *Phys. Rev. Let.* **1996**, *76*, 1541−1544.
(78) Sugawara, A.; Scheinfein, M. Room-Temperature Dipole Ferromagnetism in Linear-Self-Assembling Mesoscopic Fe Particle Arrays. *Phys. Rev. B* **1997**, *56*, R8499−R8502.